Visual Abstract

# Structural behavior of damaged reinforced concrete beams under static cyclic loading

Abdelrahman Elbaz
*University of Ain Shams, Egypt*
*Abdelrahamankhelbaz@gmail.com*

H. Marzouk, Kh. Heiza
*University of Ryerson, Canada - University of Menofiya, Egypt*
*hmarzouk@ryerson.ca, khheiza@gmail.com*

Omar Elnawawy
*University of Ain Shams, Egypt*
*nawawyomar@hotmail.com*

**ABSTRACT.** Bridges are regarded as one of the most important components of transportation infrastructure. More and more repairs, inspections, alterations, and construction processes are required to maintain safe usage due to increasing travel demands in addition to bridge infrastructure aging. In this paper, we will discuss the experimental investigation using five reinforced concrete beams to evaluate the effect of making damage to experimental beams under static cyclic loading to investigate their ductility and energy dissipation. The defective parameters taken into consideration in the experimental program were the gap in the concrete mold and mild steel at the middle bottom reinforcement. All tested specimens had the same cross-sectional dimensions. The concrete dimensions of the beams were 200 mm in width and 300 mm in height, and the beam's length was selected to be 2200 mm, having a clear span of 2000 mm between the supports, they were tested in positive bending using a 3-point bending load system. According to the results, when (RC) beams were subjected to any of the mentioned types of damage, they showed a significant decrease in ultimate capacities ranging from 3.03% to 19.31%. The ANSYS model shows an average difference with the experimental program within 4 % as acceptable agreement.

**KEYWORDS.** Monitoring, Cyclic loading, Damage Detection, Ductility, ANSYS.

OPEN ACCESS

**Citation:** Elbaz, A..KH., Marzouk, H., Heiza, Kh., Elnawawy, O., Structural behavior of damaged reinforced concrete beams under static cyclic loading, Frattura ed Integrità Strutturale, 63 (2023) 257-270.

**Received:** 04.10.2022
**Accepted:** 05.12.2022
**Online first:** 10.12.2022
**Published:** 01.01.2023

## INTRODUCTION

Bridges, towers, power generation systems, and offshore platforms are all critical structural systems in modern societies. Some of these structures are near the end of their design life and because replacing these systems is very expensive, so that the service life of these structures can go beyond the minimal service life of the design, damage detection systems are being created and applied [1]. Techniques for detecting damage in the construction of infrastructure are known as structural health monitoring (SHM) [2]. The goal of SHM is to provide a diagnosis for the condition of the various parts of the structure at each stage of its life, as well as a prediction (damage detection, residual life, and so on) [3]. Consider the first function (the diagnosis), SHM is a novel way to execute a Non-Destructive Evaluation [2]. In civil engineering, monitoring of different infrastructures, especially transportation, has become an important issue as their building and maintenance are expensive, beside the serious consequences of their sudden failure [4]. As a result, bridge SHM is almost always given special consideration. After the I-35W Mississippi River Bridge in Minneapolis, USA, collapsed in August 2007, bridge monitoring has become a crucial area of research [5]. The SHM's primary goals are to monitor the loading conditions of a structure, updating or validating the design, assessing how it performs under various service loads, identifying deterioration or damage, and providing guidance for maintenance and repairs (Xia, 2012) [6]. The twelve T-beams were evaluated for flexural behavior under cyclic load up to failure. The beams' ultimate carrying capacity was predicted using the strain compatibility technique (Honey, 2006) [7]. (A. Elshafey, 2016) [8] found the damage's location using differences in mode shape, with regard to measuring strains at high frequency rates, their findings show that the fibre bragg grating (FBG) sensor array is a quick and accurate tool. If a beam has voids, it might lose between 13 and 23 percent of its ultimate strength when subjected to a coupled load of similar quantities of flexural and torsion moments [9]. The results of the tests showed that partial unbonding of the steel-FRP composite bar (SFCB) can change or delay the failure mode while enhancing the associated deformability and energy ductility (Yunlou Sun, 2022) [10].
This paper presents a numerical and experimental analysis to assess the impact of producing damage to RC beams under static cyclic loading to assess their energy dissipation and ductility. This led to the creation of an improved method for SHM of RC beams, involving an accurate therapeutic technique for damage identification and a performance rating based on reliability.

## EXPERIMENTAL PROGRAM AND SETUP

### *Test specimens*

The test program consisted of five RC Beam specimens designed and constructed in accordance with Egyptian Concrete Code ECP 203-2007. All tested specimens had the same rectangular cross section with dimensions of 200 mm x 300 mm, with a clear span of 2000 mm between the supports. All specimens have the same configuration of longitudinal, transverse, and stirrup hanger reinforcement, with main reinforcement (2T12) and transverse reinforcement (2T10) at the top. All bars were arranged symmetrically along the beam span with a 20 mm clear cover. Fig. (1) shows the dimensions of the tested specimen beams.
The beams were cast in different condition, as given in Tab. (1). B1 is a control beam. All other beams were induced to have damage, B2 was induced to damage by placing five foam cubes with a thickness of 50mm inside the beam before casting concrete at the bottom middle span parallel with stirrup hangers for fixation. B3, B4, and B5 were induced to have mild steel at the middle of the bottom reinforcement, varying from 250mm to 1000mm, using stretch adhesive PVC cling film for food wrap at 0.008 mm thickness (plastic tape), then paint by layer of the oil to ensure that no bond between steel and concrete exists, as shown in Fig. (1).

### *Material properties*

Different reinforcement diameters were used (T12 & T10). The high tensile steel deformed rebars were used for bar sizes of 10 mm, which were used as stirrups in the transverse direction and top steel, and bar sizes of 12 mm, which were used as main steel in the longitudinal direction. The yield and ultimate strength of used bars with elongation percentage were listed in Tab. (2) according to the standard tension test.

### *Formwork*

The formwork used in the casting of the five beams was made out of timber as shown in Fig. (2), with a clear dimension of 200*300*2200 mm. Therefore, to support the weight of wet concrete without bulging in any places, the formwork must be

rigid and strong. The stiffeners were used to ensure that no distortion in the member's dimensions would occur during the casting process.

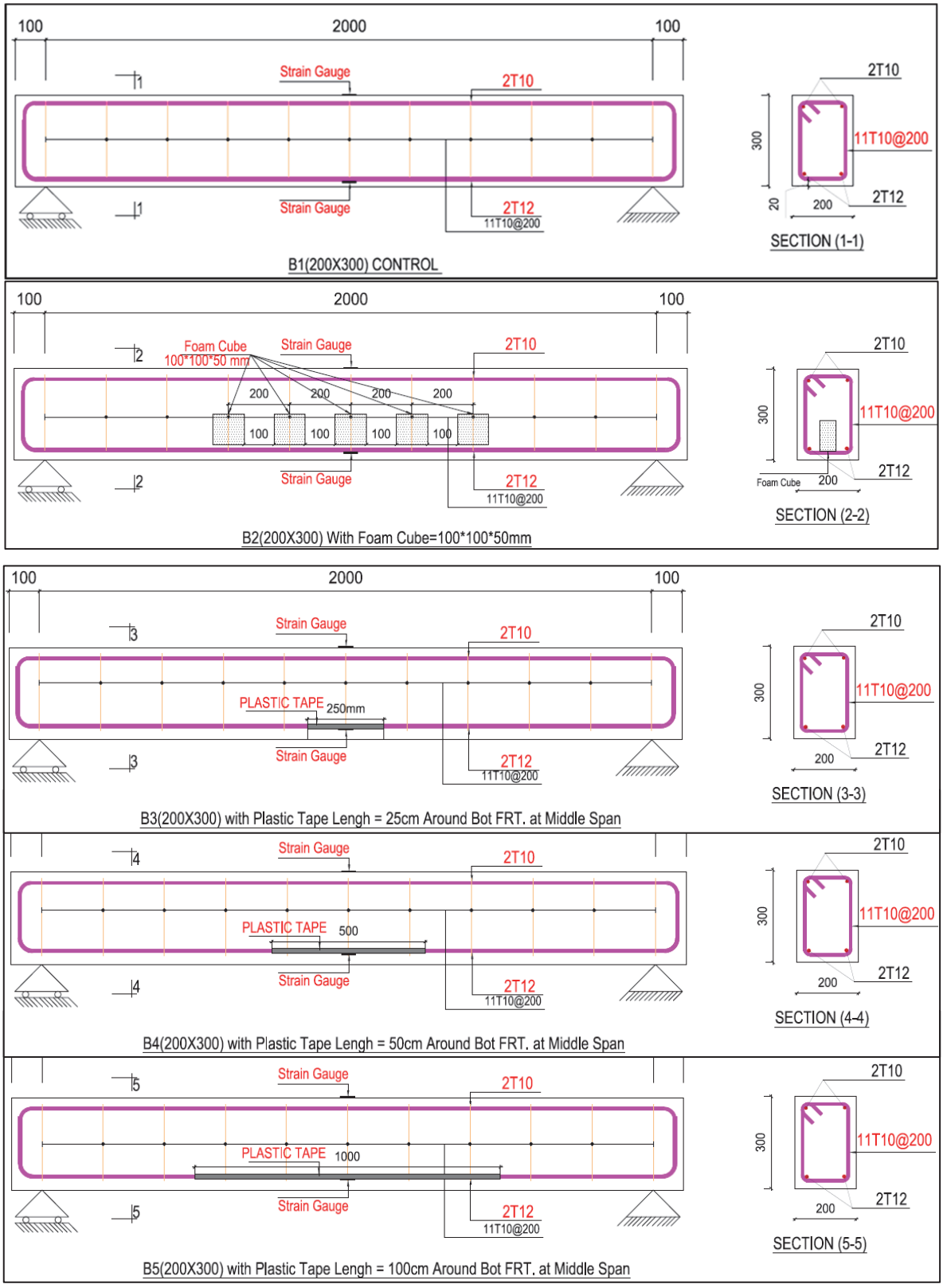


Figure 1: Dimensions of the tested beams.

| Specimen | Span (mm) | Width (mm) | Depth (mm) | Fcu (MPa) | RFT. Top | RFT. Bot. | Stirrups | Remarks |
|---|---|---|---|---|---|---|---|---|
| B1 | 2000 | 200 | 300 | 40 | 2T10 | 2T12 | T10@200 | Control |
| B2 | 2000 | 200 | 300 | 40 | 2T10 | 2T12 | T10@200 | Cube Foam 100*100*50 mm |
| B3 | 2000 | 200 | 300 | 40 | 2T10 | 2T12 | T10@200 | Mild Steel at 25 cm Mid Span |
| B4 | 2000 | 200 | 300 | 40 | 2T10 | 2T12 | T10@200 | Mild Steel at 50 cm Mid Span |
| B5 | 2000 | 200 | 300 | 40 | 2T10 | 2T12 | T10@200 | Mild Steel at 100 cm Mid Span |

Table 1: Details of experimental program tested specimens.

| Properties | High Tensile Steel (T12) | High Tensile Steel (T10) | Specification* |
|---|---|---|---|
| Yield Stress (MPa) | 556 | 547 | Min. 500 |
| Ultimate Stress (MPa) | 730.33 | 725.45 | Min. 600 |
| Weight per meter length (kg) | 0.846 | 0.592 | ---- |
| Elongation (%) | 0.215 | 0.223 | Min. 13 % |

Table 2: Properties of high tensile steel used in the experimental program.

Figure 2: Wooden formwork for specimens.

### *Concrete mix design*

The concrete used in all the experimental work had a compressive strength of 40 N/mm² after 28 days. The mixed proportions of the materials used in this research were examined in Tab. (3).

| Concrete Ingredient | | Weights (kg/m³) | |
|---|---|---|---|
| Water | | 188 | |
| Sand | | 620 | |
| Coarse Aggregate | | 1130 | |
| 3/4" | 50% | 565 | |
| 3/8" | 50% | 565 | |
| Cement | | 450 | |
| Admixture: Basef 874 high range water-reducing | | 1.8% | 8L |
| Admixture: Basef 875 Superplasticizer | | 0.3% | 1.2L |

Table 3: Concrete mix proportions /m³.

*Induced Damage*

For beam B2, five foam cubes with dimensions of 100 mm x 100 mm x 50 mm were installed with stirrup huggers by steel wire to ensure that they remained fixed in place after concrete casting, as shown in Fig. (3). B3, B4, and B5 were induced to have mild steel at the middle of the bottom reinforcement, varying lengths from 250mm to 1000mm, covered by stretch adhesive PVC cling film for food wrap, 0.008 mm thickness (plastic tape), then painted with a layer of oil to ensure the smoothness of the steel bar and no friction with concrete, as shown in Figs. (4 and 5).

Figure 3: Overview of size and fixation of embedded foam cube.


Figure 4: Process of steel isolation wrapping and painting.

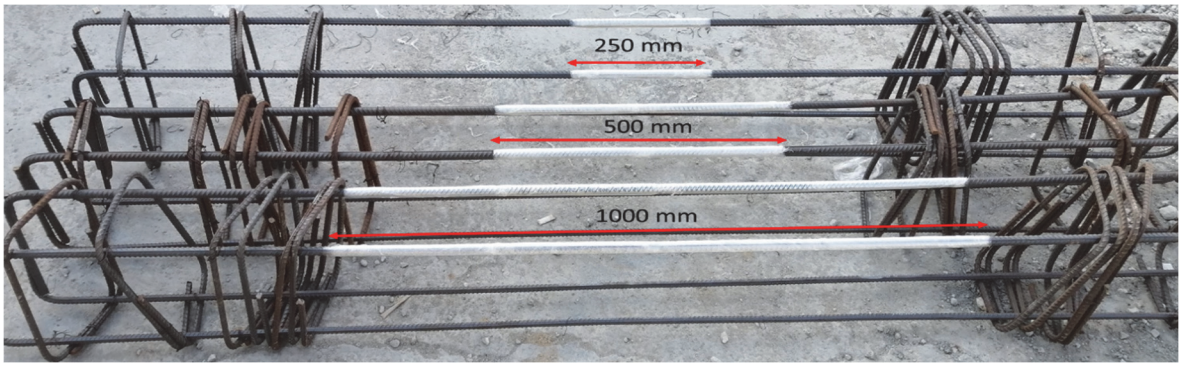


Figure 5: Final isolation of bottom steel from 250 to 1000 mm.

*Fabrication*

At first, the reinforcement was prepared according to the details stated in Tab. (1) as shown from Fig. (1). For B2, five foam cubes were installed at the middle bottom of the beam as shown in Fig. (3). Plastic tape was wrapped around the middle bottom reinforcement of beams B3, B4, and B5, before installing reinforcement inside the form work, and then painted with an oil layer after the form work was installed, as shown in Fig. (4). To measure the strain of the main reinforcement,

strain gauges were attached at mid span as shown in Fig. (6). The reinforcement was installed inside each formwork for specimens and adjusted to provide a concrete cover of 20 mm in all directions.
The formworks were sprayed with water before the concrete was cast, and then reinforcements were placed in their right positions in the forms. Just after mixing, the concrete was poured into wood forms and compacted with a vibrating machine for 1 minute for good compaction of the concrete, as shown in Fig. (7).
All beams were cast in the formwork on the same day and from the same concrete batch. The beams were removed from the formworks after three days from the time of the concrete cast. Burlap was then used to cover the specimens. All the beams were tested after 28 days from the time of concrete casting.

Figure 6: Installation of strain gauge and using tools.

For control purposes, six standard cubes and six standard cylinders were prepared and coated with oil before casting, and then concrete was placed after mixing in three layers, each layer compacted by 25 blows with standard rods according to the British Standard Specification (B.S.1881) and tested on the same day as the beams. The concrete cylinders and the concrete prisms were cast on the same day using the same concrete mixes described before. Finally, the specimens were white washed and then removed for storage on the day of testing.

Figure 7: Beams specimens during and after casting.

*Compressive strength test*

The goal of this test was to determine the concrete cube specimens' compressive strength (Fcu). To conduct this test, molded cubes were subjected to a compressive axial load until failure. By dividing the maximum load achieved during the

test by the specimen's cross-sectional area, the Fcu of the specimen was determined. A 3000 kN capacity compression testing machine was used. The cubes were tested at two different dates as follows:
a) Three were emerged in water and tested after 7 days
b) Three were emerged in water and tested after 28 days
The test was conducted on 6 cubes measuring (150* 150* 150) $mm^3$. The data was recorded and the average 28-day concrete strength was 46.26 MPa. Tab. (4) displays the compressive strength of concrete at various testing dates.

| Age | Fcu (MPa) | Average Fcu (MPa) |
|---|---|---|
| 7-days | 39.7 | 36.36 |
| | 38.5 | |
| | 30.9 | |
| 28-days | 48.8 | 46.26 |
| | 49.7 | |
| | 40.3 | |

Table 4: Concrete compressive strength.

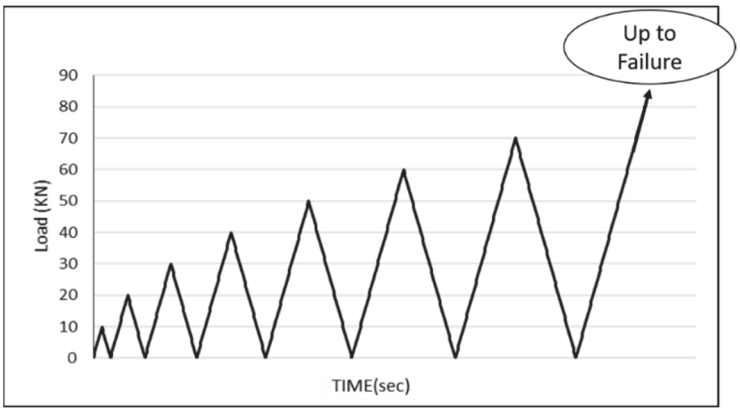


Figure 8: Pattern static cyclic loading.

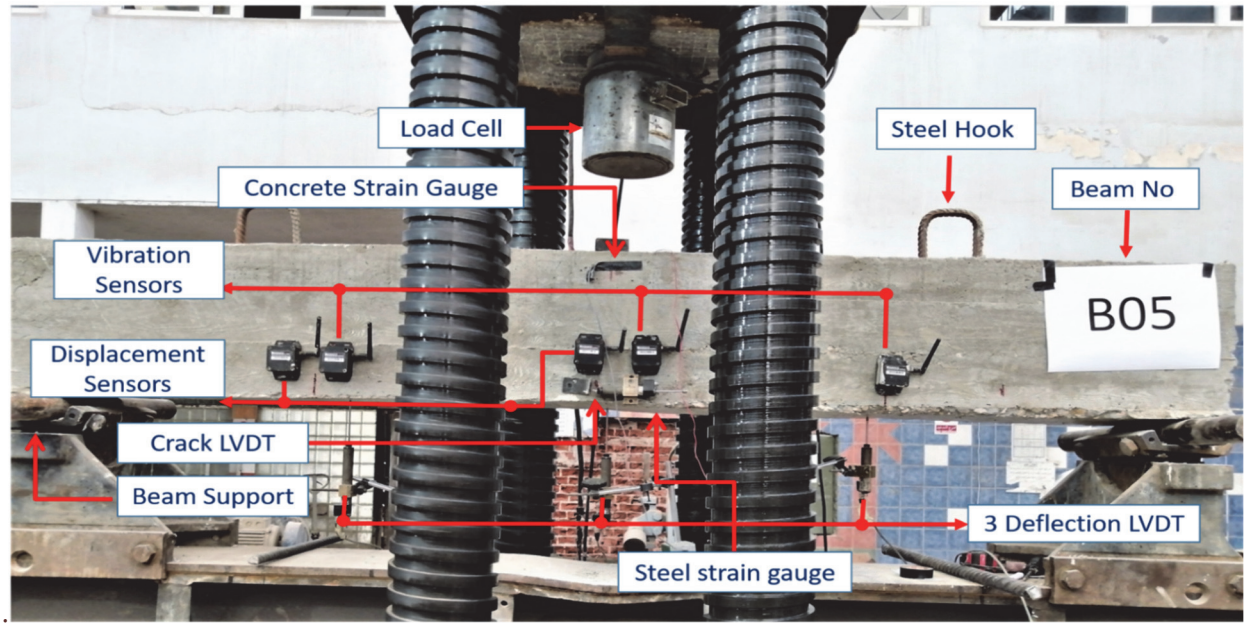


Figure 9: Beams under testing

*Test setup and loading scheme*

The experiments were carried out at Egypt's Housing and Building National Research Center (HBRC) Institute. The beams were tested under static cyclic loading until failure. A one-point concentrated load at 1100 mm from the beam edge was

applied using a load cell incremental system. In order to equally distribute the load, a steel plate was put under the point load, as shown in Fig. (9). The static cyclic loading was achieved by increasing the load from zero KN up to 10 KN gradually with a constant rate of loading during the test, then freeing the load cell back to zero and repeating this cycle from zero KN up to 20 KN and so on by increasing 10 KN in each cycle as shown in Fig. (8), with the following loading and unloading technique to beam failure. The data was gathered at a rate of one sample per second using a data acquisition system. Two strain gauges were used in order to record the strains in the concrete and reinforcing bars at each load stage. After preparing the test setup and before loading, zero loading of strains and vertical concrete displacements were recorded and checked. To gauge the beams' vertical deflection, three linear variable displacement transducers (LVDT) were used as seen in Fig. (9), the first one was located in the center of the beam, whereas the others were spaced a quarter of a span from the left and right edges. The crack gauge was used to measure the breadth of the crack at the beam's midspan. When the tests were conducted, color markers were used to mark the specimen's cracks once they had been tracked throughout its sides. Each specimen's first cracking load was recorded and the load was gradually increased up to failure.

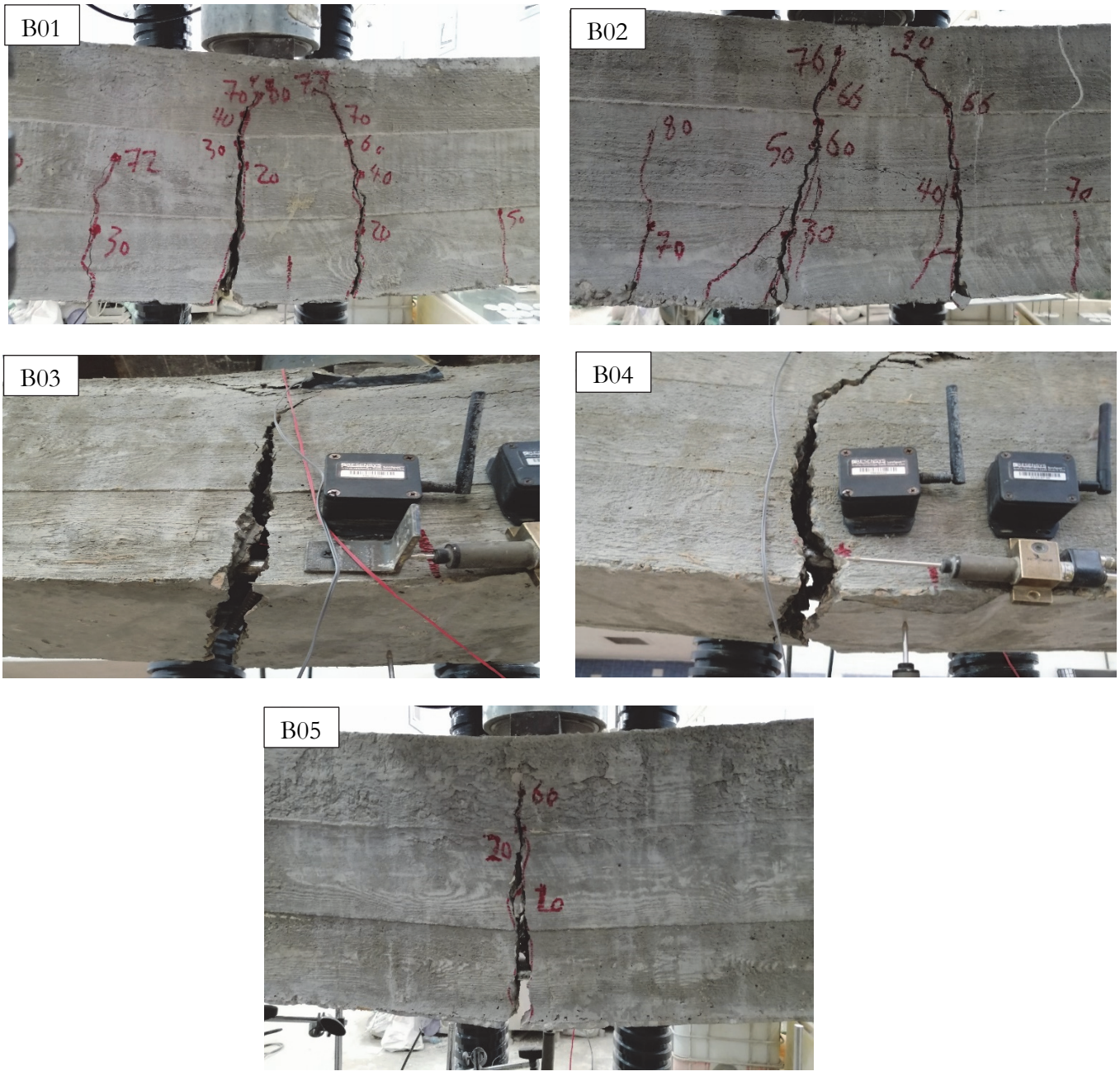


Figure 10: Modes of failure for all tested specimen.

## EXPERIMENTAL RESULTS AND DISCUSSION

The results of the experimental program are summarized in Tab. (5); namely, the load and deflection at which the first cracks start (Pcr and Δcr), the yielding load and deflection (Py and Δy), the maximum load and deflection (Pmax and Δmax), maximum strain at tension reinforcements (ε), stress at tension reinforcement, maximum crack width, maximum strain at compression (ε) and failure mode for each beam according to crack patterns. Fig. (10) shows the mode of failure for all tested specimens under static cyclic loading.

### *Effect of voids on the load versus mid span deflection*

Fig. (11) depicts the load against mid-span deflection responses for tested beams B1 and B2. From the same figure and Tab. (5) by comparing the results of control beam (B1) with beam (B2), it was observed:

- The load carrying capacity of the tested beam (B2) which was induced by having a void in the concrete mold before concrete casting, decreased by 7.6 % compared to the control beam (B1).

Conclusion: Having voids in a concrete mold reduces the ultimate load and stiffness of flexural tested beams.

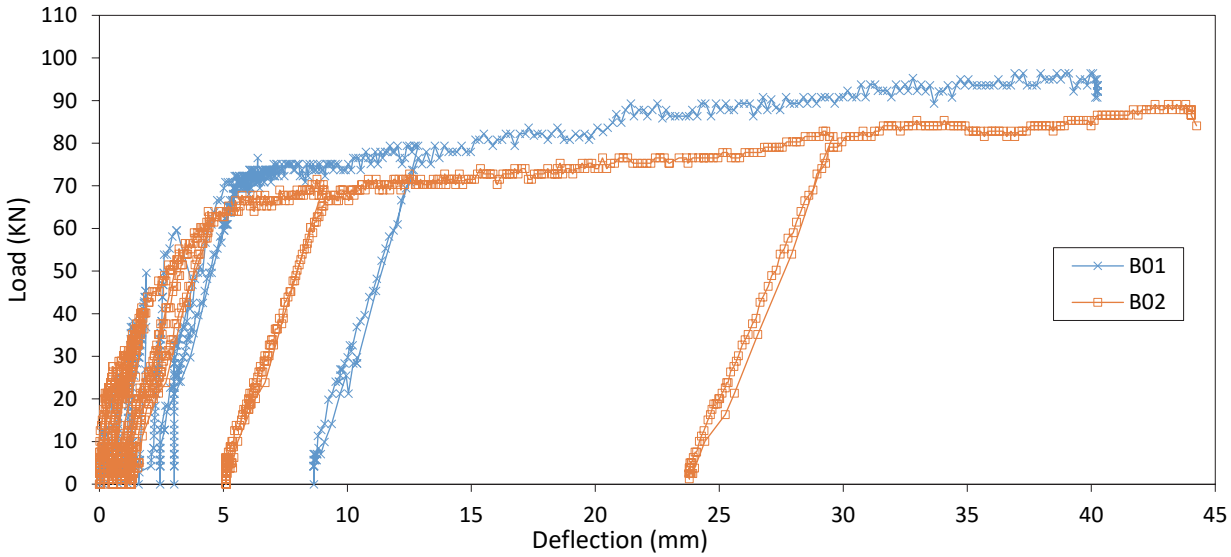


Figure 11: Load deflection curves for beams (B1 and B2).

### *Effect of mild steel on the load versus mid-span deflection*

Fig. (12) shows the load versus mid-span deflection responses for tested beams (B1, B3, B4 and B5).

From Fig. (12) and Tab. (5) by comparing the results, it was observed:

- The load carrying capacity of the tested beam (B3) induced by having a mild steel at the middle bottom reinforcement with a length of 250mm decreased by 8.9 % compared to the control beam (B1).
- The load carrying capacity of the tested beam (B4) induced by having a mild steel at the middle bottom reinforcement with a length of 500mm decreased by 13.82 % compared to the control beam (B1).
- The load carrying capacity of the tested beam (B5) induced by having a mild steel at the middle bottom reinforcement with a length of 1000mm decreased by 19.31 % compared to the control beam (B1).

Conclusion: Increasing the length of mild steel at the middle bottom of the reinforcement reduces stiffness and ultimate load of flexural tested beams.

### *Ductility*

Each design code is aware of the importance of ductility in design because a ductile structure can absorb more energy without completely collapsing. The test results demonstrate that when RC beams are damaged in any way, such as what was mentioned in our research, their ultimate capacities will significantly decrease. However, as the beams' load-deflection curves show, the gains in capacity are usually at the expense of ductility (Oudah 2012) [11].

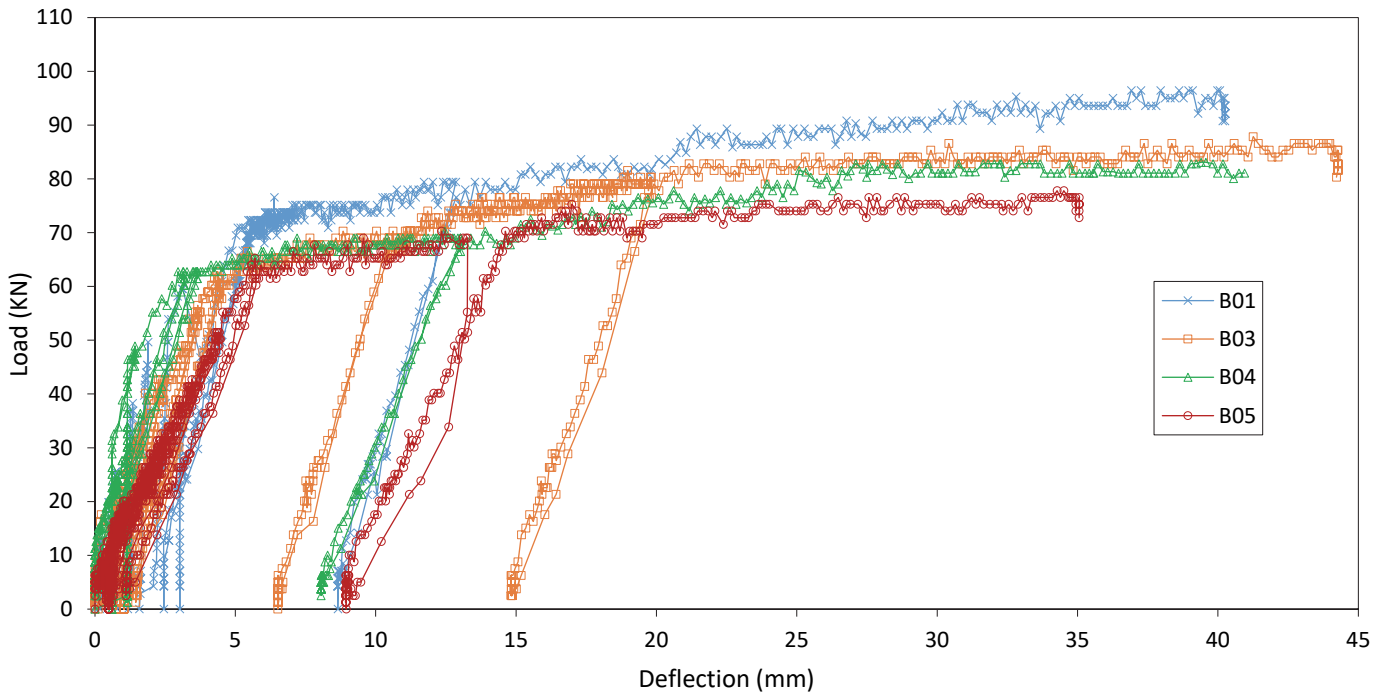


Figure 12: Load deflection curves for beams (B1, B3, B4 and B5)

| Beam | Cracking Stage | | Failure Stage | | Maximum strain at tension RFT (ε)(mm/mm) | Maximum strain at Concrete (ε)(mm/mm) | Maximum Crack Width (mm) | Mode of Failure |
|---|---|---|---|---|---|---|---|---|
| | Pcr (kN) | Δcr (mm) | Pmax (kN) | Δmax (mm) | | | | |
| B1 | 20 | 0.617 | 96.434 | 36.911 | 0.040527 | 0.001276 | 10.552 | Ductile Flexural Failure |
| B2 | 30 | 1.201 | 89.1 | 42.574 | 0.031313 | 0.001854 | 12.262 | |
| B3 | 10 | 0.124 | 87.85 | 41.256 | 0.03321 | 0.001054 | 19.637 | Pure Flexural Failure |
| B4 | 10 | 0.607 | 83.1 | 39.397 | 0.01932 | 0.001306 | 26.405 | |
| B5 | 10 | 0.259 | 77.81 | 34.512 | 0.010005 | 0.002098 | 28.343 | |

Table 5: Experimental results and modes of failure

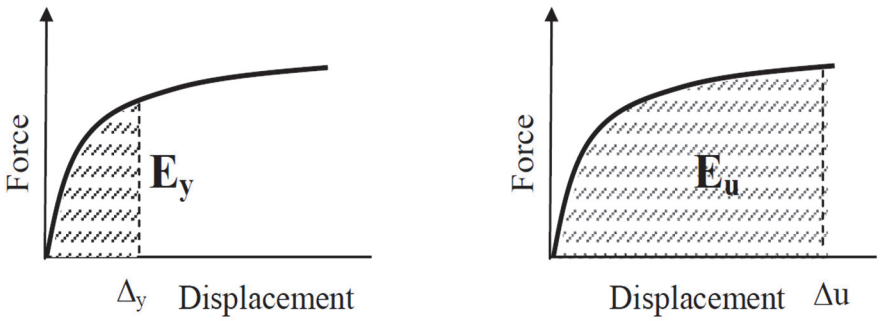


Figure 13: Definition of ductility index.

Deflection ductility: $$\mu_{\Delta} = \frac{\Delta_u}{\Delta y} \quad (1)$$

Energy ductility: $$\mu_E = \frac{Eu}{Ey} \quad (2)$$

$$Ductility\ ratios = \frac{ductility\ ofdamaged\ beam}{ductility\ of\ control\ beam} \quad (3)$$

The results of the ductility are summarized in Tab. (6). Deflection ductility $(\mu_{\Delta})$ is defined in Eqn. (1) as the ratio of displacement at failure $(\Delta_u)$ to displacement at yield $(\Delta_y)$, whereas energy ductility $(\mu_E)$ is defined in Eqn. (2) as the ratio of energy at failure (Eu) to energy of the first steel yield (Ey), then the ductility ratio can be calculated as in Eqn. (3). It can be concluded that any type of failure in RC beams must result in significant ductility gain, especially if the failure mode is premature, such as debonding or flexure failure.

| Beam | Ductility | | Ductility ratio | |
|---|---|---|---|---|
| | In terms of deflection (μΔ) | In terms of energy (μE) | In terms of deflection (μΔ) | In terms of energy (μE) |
| B 1 | 5.99 | 10.17 | 1 | 1 |
| B 2 | 8.58 | 13.29 | 1.43 | 1.31 |
| B 3 | 8.83 | 15.21 | 1.47 | 1.5 |
| B 4 | 9.74 | 14.68 | 1.63 | 1.44 |
| B 5 | 5.62 | 9.15 | 0.94 | 0.9 |

Table 6: Ductility index for tested beams.

## VERIFICATION STUDY

The verification that follows provides a description of finite element (FE) models using (ANSYS 2021 R2) used to estimate the modes of failure and load-deflection behavior for the tested RC beams mentioned above subjected to static cyclic loading. The Tab. (7) lists the mechanical characteristics of foam-filled voids, steel bars (T12&T10), and concrete. The element SOLID65 is used to model the concrete in its form. This element can crack, deform, and crush in three orthogonal directions. Two different types of reinforcement bars were used to create the FE models for the beams in accordance with the results of uni-axial tensile tests. The meshing of concrete, steel reinforcement, supports, plate of loading and the foams which fill the voids for specimen (B2) are shown in Figs. (14 and 15).

| Material | FE type | Density(kg/cm²) | Elastic modulus (MPa) | Passion's ratio | Fcu (MPa) | Fy (MPa) |
|---|---|---|---|---|---|---|
| Concrete | SOLID 65 | 2500 | 29800 | 0.2 | 46 | |
| Steel (T12) | LINK 180 | 7850 | 200000 | 0.3 | | 556 |
| Steel (T10) | LINK 180 | 7850 | 200000 | 0.3 | | 547 |
| Steel Plate | LINK 185 | 7850 | 200000 | 0.3 | | |
| Foam | | 100 | 107 | 0.3 | | |

Table 7: mechanical Prop. of used materials.

### *Numerical versus experimental results*

Tab. (8) compares the numerical and experimental results obtained for all specimens examined for both the cracking stage and the failure stage and demonstrates how to model the static cyclic loading behavior of RC beams using the numerical method discussed here. It is shown that the results for the five beams obtained from the FE model agree with the results obtained from the experimental results. At both the intact and damaged states, the average difference between the experimental and FE model values of ultimate capacity is less than 4%.

An examination of Tab. (8) reveals that:
The FE results closely match the outcomes of the experiment; the first cracking loads from the FE analyses and the experimental data are almost comparable, as seen in Tab. (8). This is possibly due to the sensitivity of the numerical solution to concrete and reinforcement constitutive stress-strain curves in the nonlinear period.

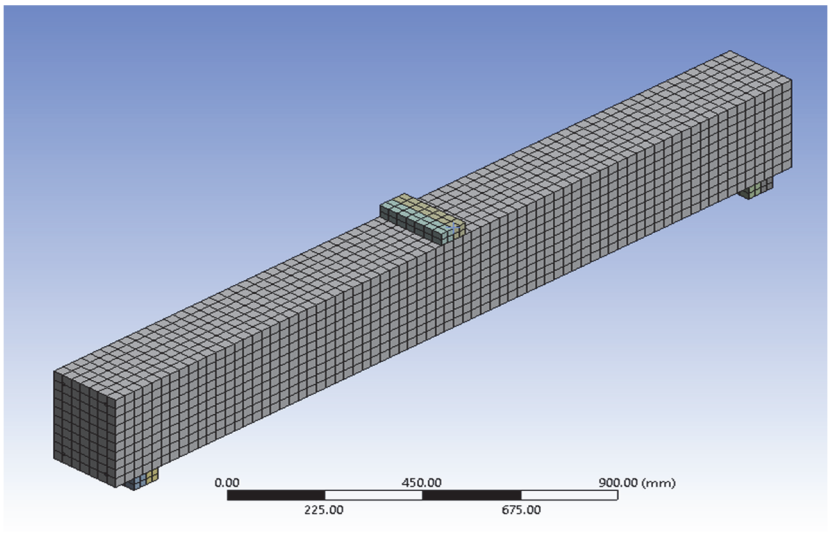


Figure 14: FE meshes for the tested beams

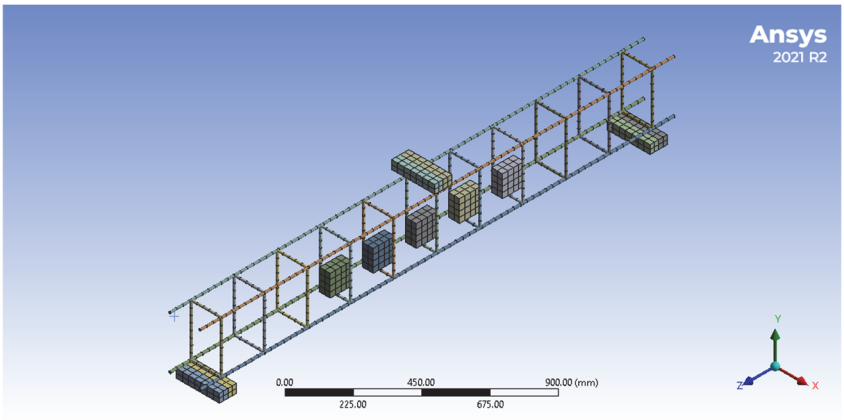


Figure 15: FE meshes for voids at B2

Fig. (16) compares the failure loads of the experimental and final loads from the FE models, and it displays the load plots from the FE analyses for all beams at the last converged load step. Fig. (17) displays the deflection plots from all beams at the maximum load step from the FE analyses and compares the maximum deflection from the FE models with the maximum deflection from the experiments.

| Beam | Cracking Stage | | | | Failure Stage | | | | Pmax (exp)/ Pmax (num) |
|---|---|---|---|---|---|---|---|---|---|
| | EXP. | | FEM | | EXP. | | FEM | | |
| | $P_{cr}$ (KN) | Δcr (mm) | $P_{cr}$ (KN) | Δcr (mm) | $P_{max}$ (KN) | Δmax (mm) | Pmax (KN) | Δmax (mm) | |
| B1 | 20 | 0.617 | 18.759 | 0.232 | 96.43 | 36.911 | 97.102 | 44.915 | 0.9931 |
| B2 | 30 | 1.201 | 13.566 | 0.444 | 89.10 | 42.574 | 88.232 | 27.764 | 1.0098 |
| B3 | 10 | 0.124 | 17.545 | 0.876 | 87.85 | 41.256 | 90.697 | 45.310 | 0.9686 |
| B4 | 10 | 0.607 | 19.221 | 0.239 | 83.10 | 39.397 | 84.878 | 44.298 | 0.9791 |
| B5 | 10 | 0.259 | 14.397 | 0.563 | 77.81 | 34.512 | 80.965 | 40.448 | 0.9610 |

Table 8: comparing the results of experiments with numerical.

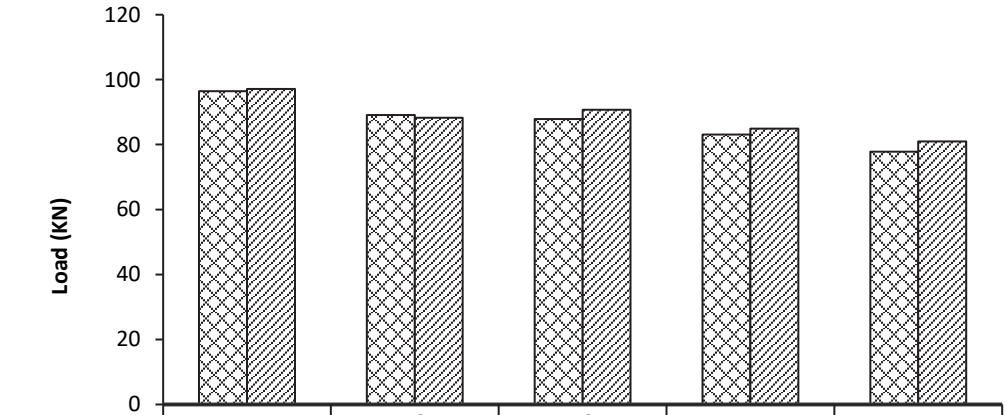


| | B1 | B2 | B3 | B4 | B5 |
|---|---|---|---|---|---|
| Pmax (exp.) | 96,434 | 89,1 | 87,85 | 83,1 | 77,81 |
| Pmax (num.) | 97,102 | 88,232 | 90,697 | 84,878 | 80,965 |

Figure 16: Comparisons between failure loads of the experimental and FE final loads for all beams.

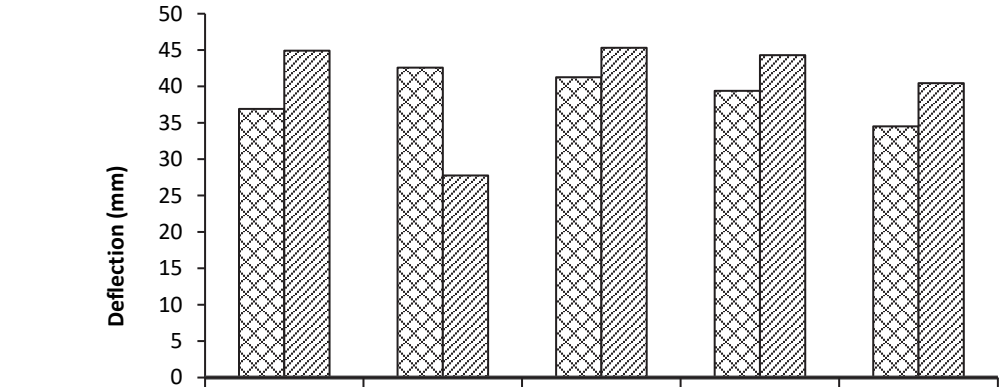


| | B1 | B2 | B3 | B4 | B5 |
|---|---|---|---|---|---|
| Max DEF. (exp.) | 36,911 | 42,574 | 41,256 | 39,397 | 34,512 |
| Max DEF. (num.) | 44,915 | 27,764 | 45,31 | 44,298 | 40,448 |

Figure 17: Comparisons between max deflection of the experimental and FE for all beams.

## Conclusions

- The ultimate capacity of the tested beam (B2) induced by damage presented as a gap in the concrete mold decreased by 7.6% compared to the control beam (B1). It can be concluded that the presence of voids in the concrete mold decreases the ultimate load and the tensile steel strain while it increases the deflection and concrete compressive strain.
- The ultimate capacity of tested beams (B3, B4 and B5) induced by having a mild steel at middle bottom reinforcement with variable length from 250 mm to 1000 mm decreased by 8.9 %, 13.82% and 19.31% respectively than control beam (B1). It can be concluded that increasing mild steel length at middle bottom reinforcement decreases the ultimate load, stiffness, deflection and the tensile steel strain while it increases the concrete compressive strain of static cyclic loading tested beams.
- It is essential that RC beams which are subjected to any type of failure result in significant ductility gain, mainly if the failure mode is premature, such as debonding or flexure failure.
- The numerical results of the tested specimens demonstrated similar key conclusions to the experimental ones; the finite element models are shown to accurately predict the structural behavior of RC beams under static cyclic loading deviations varying no more than 4 % for all specimens.

- Finally, a high-risk limit that necessitates rapid repair or replacement of the deteriorating structural member to avoid catastrophic failure. These limitations on performance evaluation are adequate for monitoring RC structures and providing trustworthy performance evaluations for any decision-making process.

## REFERENCES

[1] Farrar, Charles R., and Keith Worden. (2012). Structural health monitoring: a machine learning perspective, United Kingdom, John Wiley & Sons, IBSN: 978-1-119-99433-6.

[2] Farrar, Charles R., and Keith Worden. (2007). An introduction to structural health monitoring. Philosophical Transactions of the Royal Society of London A: Mathematical, Physical and Engineering Sciences 365(1851), pp. 303-315.

[3] Fritzen, C.-P., Balageas, D. and Güemes, A. (2010). Structural health monitoring, 90, John Wiley & Sons, IBSN 13: 978-1-905209-01-9.

[4] González, I. (2011). Study and application of modern bridge monitoring techniques, Sweden, Universitets service US-AB. ISSN 1103-4270.

[5] Chowdhury, F. H., Raihan, M. T. and Islam, G. M. S. (2015). Application of different structural health monitoring system on bridges, Conference on Advances in Bridge Engineering-III, Dhaka, Bangladesh.

[6] Xu, Y. L., Zhang, X. H., Zhan, S., Hong, X. J., Zhu, L. D., Xia, Y., & Zhu, S. (2012). Testbed for structural health monitoring of long-span suspension bridges. Journal of bridge engineering, 17(6), pp.896-906.

[7] Abd. Hosny, H. Shahen, A.abd, and T. Elafandy (2006). Performance of reinforced concrete beams strengthened by hybrid FRP laminates, cement and concrete composites, 28(10), pp. 906-913. ISSN: 0958-9465.

[8] Elshafey, A., Marzouk, H., Gu, X., Haddara, M., Morsy, R. (2016). Use of fiber Bragg grating array and rand decrement for damage detection in steel beam, Engineering Structures, 106, pp. 348–354.

[9] Ajeel, A. E., Qaseem, T., Rasheed, S. (2018). Structural behavior of voided reinforced concrete beams under combined moments, Civil and Environmental Research, 10, pp. 17–24.

[10] Sun, Y., Fu, J., Sun, Z., Zhang, J., Wei, Y., Wu, G. (2022). Flexural behavior of concrete beams reinforced by partially unbonded steel-FRP composite bars, Engineering Structures, 272, 115050.

[11] Oudah, F. and El-Hacha, R. (2012). A new ductility model of reinforced concrete beams strengthened using fiber reinforced polymer reinforcement. Composites Part B: Engineering, 43(8), pp. 3338-3347.